ANALYSIS OF DYNAMIC CRACK GROWTH BASED ON MICROMECHANICAL MODELS

D.-Z. Sun*, A. Hönig*, W. Schmitt*

Two strain-rate dependent material models based on the modified Gurson flow function are compared by simulating different specimens loaded dynamically. The influences of strain rate on the critical volume fraction of voids and on the characteristic distance are investigated. The material parameters for the micromechanical models are obtained from the simulation of dynamic tension tests and CT-specimen. The transferability of the material models and the damage parameters is checked by modeling a SENB specimen. The measured static and dynamic J_R-curves are compared with those calculated using the micromechanical models. An attempt has been made to determine the material parameters from the Charpy-V specimen. A combination of plane strain and plane stress conditions is assumed to model the Charpy-V specimen.

INTRODUCTION

The safety analysis of components loaded dynamically requires the description of the strain-rate dependence of the material hardening and the introduction of fracture criteria. The effects of strain-rate and temperature on strength and toughness were investigated in a wide range for different steels (1,2). The corresponding material laws for the strain-rate hardening base either on models taking account of microscopic slip processes or on empirical description (3,4). However, one finds only a few numerical studies which prove the applicability of different material laws by modeling specimens or components under dynamic loading. The effect of the adiabatic softening is rarely included in such simulations. In analyses of dynamic ductile crack growth the J-integral or the crack-tip-opening displacement CTOD have been widely used. But the strain-rate dependence and geometry dependence of the crack resistance curves make the application of these concepts difficult. As an alternative a micromechanical model was used by Needleman and Tvergaard (5) to study dynamic ductile crack growth in a double edge cracked specimen. The results computed on the basis of the micromechanical model were not checked by experimental investigations. However, some papers give evidence that this type of the micromechanical model describes the fracture behaviour of material very well (6,7), at least in the case of static loading.

* Fraunhofer-Institut für Werkstoffmechanik, Freiburg, Germany

The aim of the present work is to check the applicability of micromechanical models for dynamic loading. Both a theoretical and an empirical strain-rate dependent material model were implemented in a commercial finite element program based on the modified Gurson model. The parameters for the strain-rate hardening and the damage models were determined by simulating the smooth tension specimen and applied to model the impact Charpy-V and SENB specimens. The static and dynamic J_R-curves computed using the micromechanical models were compared with the experimental ones.

STRAIN-RATE DEPENDENT MODELS

According to Macherauch and Vöhringer (8) the yield stress, σ_y, can be seperated into a thermally inactive part, σ_i, and a thermally activated part:

$$\sigma_y = \sigma_i + \sigma_o^* \left[1 - \left[\frac{kT}{\Delta G_o} \ln \frac{\dot{\varepsilon}_o}{\dot{\varepsilon}_p}\right]^q\right]^p \qquad (1)$$

with k the Boltzmann constant, T temperature and $\dot{\varepsilon}_p$ the actual plastic strain rate; p, q, ΔG_o, $\dot{\varepsilon}_o$ and σ_o are material constants. σ_i is determined by the interaction between the dislocations and long range stress field caused by grain boundaries, second phases and precipitations. In contrast to σ_i the thermally activated part of the yield stress is given by the interaction between the dislocations and short range stress like Peierls-Nabarro stress. Thermal activation processes help the dislocations to overcome these short range obstacles. The flow stress σ consists of the yield stress and the contribution of the plastic strain hardening σ_d:

$$\sigma = \sigma_y + \sigma_d(\varepsilon, T) \qquad \text{(model 1)} \qquad (2)$$

A simple empirical approximation of the flow stress σ has been introduced by Pan et al. (9):

$$\sigma = \sigma_G(\varepsilon, T) \left[\frac{\dot{\varepsilon}_p}{\dot{\varepsilon}_o}\right]^m, \quad m << 1 \quad \text{(model 2)} \qquad (3)$$

$\dot{\varepsilon}_o$ is a reference strain rate and σ_G denotes the flow stress measured at the reference strain rate.

During the plastic deformation nearly all the plastic work is converted into heat. If the deformation takes place slowly, the heat generated within the specimen can flow to the surrounding and the temperature of the specimen will not change. A test under this conditions is considered isothermal. On the other side, if the strain rate in a test exceeds a critical strain rate, the heat transfer during the deformation is negligible. This type of tests is called adiabatic. The temperature increase for an adiabatic test can be calculated from the energy balance:

$$\Delta T = \frac{\chi}{\rho\, c_p} \int \sigma_{ij} \cdot d\varepsilon^p_{ij} \qquad (4)$$

where ρ and c_p are density and heat capacity respectively. The typical value of the parameter χ is (for metals) 0.9 (5). The adiabatic heating results in softening of material due to the reduction of the yield stress and the decrease of the plastic hardening. If the temperature increment calculated with equation 4 is inserted in equation 1 and 2, the adiabatic softening is naturally described by model 1. For model 2 the temperature dependence of the flow stress has to be introduced directly. According to (5) a linear relationship between the flow stress and temperature is assumed:

$$\sigma_G(\varepsilon, T) = \sigma_G(\varepsilon, T=T_o)\ [1-\beta\ (T-T_o)] \qquad (5)$$

where β is a material dependent parameter.

Both strain-rate dependent models have been introduced into the modified Gurson model (5-7) and implemented in a commerical finite-element program. In the micromechanical model the rupture is a natural result of the void coalescence which begins when a critical void volume fraction f_c is exceeded over a characteristic distance l_c. To increase the stability and accuracy of the finite-element calculation the plastic strain rate $\dot{\varepsilon}_p$ and the stiffness matrix are calculated with a semi-implicit formula after Peirce et al. (10). The stresses and internal variables are integrated with a 4th-order Runge-Kutta method.

VALIDATION OF THE MODELS

To check the strain-rate dependent material models and to determine the critical void volume fraction f_c, the smooth tensile specimens were simulated for static and dynamic loads. Since in the smooth bar the distribution of stresses and void volume fraction over the cross section is fairly homogeneous, the damage parameter f_c can be evaluated without taking into account a characteristic distance l_c. The experiments were carried out with the pressure vessel steel 22 Ni Mo Cr 3 7 (≙ ASTM A 508 Cl 2). The diameter and the length of the tensile specimens are 6 mm and 30 mm respectively. The specimens were loaded with a plastic strain rate $\dot{\varepsilon} = 1.6 \cdot 10^{-4}$/s in the quasi-static tests and $\dot{\varepsilon} = 40$/s in the dynamic tests. After maximum load the strain rates increase by about a factor of 10.

For model 1 three parameters ($p = 3$, $q = 1$, $\sigma_i = 350$ MPa) were fixed considering results of (2). The remaining parameters $\Delta G_o = 2.10^{-19}$ J, $\dot{\varepsilon}_o = 5.58 \cdot 10^4$/s and $\sigma_o = 423$ MPa were determined using the yield stresses measured at room temperature under static and dynamic loadings and the static yield stress at the temperature of 493 K. For model 2 the parameter $m = 0.0175$ was obtained by inserting the stresses at maximum loads and the corresponding strain rates into equation 3. To calculate the adiabatic heating $c_p = 465$ J/(kg K) and $\rho = 7800$ kg/m^3 were used. The value $\beta = 0.004$/K was evaluated from the static yield stresses measured at two different temperatures (293 K, 493 K).

Figure 1 shows the numerical and experimental load vs. diameter change curves (11) obtained from the smooth bar under static and dynamic loadings. The static experimental results are in good agreement with the curve calculated using model 2 ($m = 0.0032$) in combination with the modified Gurson model. The critical void volume fraction $f_c = 0.045$ is determined by fitting the sudden drop in the static load vs. diameter change curve. This f_c-value was also used for all simulations of the dynamic tests. The dynamic deformation behaviour of the tensile bar is well described by model 2 with both isothermal and adiabatic conditions up to maximum load and after that the results computed under the isothermal condition deviate more and more from the experimental data. The calculation taking into account the adiabatic softening with the measured parameter $\beta = 0.004/K$ delivers an improved result. However, a good agreement between the numerical and experimental results can only be obtained by changing the parameter β to $0.008/K$ which is the double of the measured value. Similar results were also obtained using model 1 on the assumption that the part of the flow stress σ_d caused by plastic hardening is not influenced by the strain rate and temperature (12). From the simulations it can be concluded that the adiabatic softening is not the only reason for the reduction of the dynamic flow stress with increasing plastic deformation. An improved description of the dynamic tensile tests by model 1 can be expected, if the effects of the strain rate and temperature on the plastic hardening are not neglected. A systematic study on these effects has to be carried out both experimentally and numerically. However, since large plastic strain appears only in a small region of complex specimens, the softening effects observed in the dynamic uniaxial tension test do not play an essential role in those cases. Figure 1 also indicates that the final rupture of dynamic tensile specimens is predicted in a satisfactory way with different computations. This means that the critical void volume fraction f_c is not very sensitive to strain rate.

MODELING OF THE SENB AND CHARPY-V SPECIMENS

To check the transferability of the material models and the damage parameters to different specimen geometries and strain rates a precracked Charpy specimen (SENB 10) of a test series described by Böhme (13) was modelled. The SENB specimen has 20 % side grooves and a relative crack length of $a/W = 0.53$. The simulation was performed under assumption of plane strain conditions using the same material parameters as for the simulation of the dynamic tensile tests. The unknown parameter, l_c, was determined by matching the calculated load vs. displacement curve with the experimental curve of a sidegrooved CT-specimen under quasi-static loading. The applied l_c-value is 0.1 mm, which is identified with the length of the elements at the crack tip. The supports of the specimen were modelled as contact surfaces. Figure 2 shows that the measured load vs. displacement curve of the SENB specimen is in good agreement with the numerical curves calculated using model 2 with the isothermal conditions and model 1 with the adiabatic conditions. In contrast to the smooth tensile specimen the adiabatic effect in the SENB specimen is negligible.

Figure 3 shows the calculated and measured J_R-curves for static and dynamic loadings. Obviously, the difference between the numerical and expe-

rimental J_R-curves increases with increasing Δa-value. To find out the reason for this discrepancy the Δa-values measured with the multi-specimen method were compared with the values calculated using the micromechanical model. It was found that the crack extensions were predicted in a very satisfactory way. This means that the difference between the numerical and experimental J_R-curves is only attributed to the evaluation of the J-values. It is also supported by the finding that in the simulation a strong path dependence of the J-integral is determined at large crack extension. One possible reason for the discrepancy between the numerical and experimental results is the violation of the conditions the J-controlled crack extension. However, the problem of validity for the J-integral can not simply be solved by increasing the size of specimens, since in the larger samples of the material, side cracks appear (13). The exact prediction of the load vs. displacement curve and the crack extension by the micromechanical model implies that in contrast to the J-integral concept the damage model can be applied also to describe large crack extension in small specimens.

The Charpy-V-notch impact test is one of the most frequently used test procedures and many attempts have been made to correlate information of the Charpy test with fracture toughness values or (J)-resistance curves on a more or less empirical basis. In this study a Charpy-V specimen was modelled using the modified Gurson model to obtain the micromechanical material parameters in analogy to the procedure for the tension test. Since the standard Charpy-V specimen is not sidegrooved, the state of stress in the specimen can not be approximated with plane strain conditions everywhere. As shown in figure 4, the assumption of plane strain results in a considerable overestimation of the applied load before crack initiation and a sudden drop of the load after the critical void volume fraction $f_c = 0.045$ is exceeded locally. The load vs. displacement curve calculated under the assumption of plane stress is close to the experimental curve before the measured maximum load is reached. As the f_c-value of 0.045 determined from the tensile specimen is not reached in the simulation based on plane stress conditions and therefore no crack extension is modelled in the numerical analysis, the computed load vs. displacement curve deviates from the measured one after the crack initiation. According to Riedel (14) a plane strain field exists at the crack tip only over a finite range and it is independent of whether the overall specimen response is closer to plane stress or plane strain. The size of the plane strain field can be evaluated numerically. An approximate analysis for linear viscous material shows that the range of the plane strain field on the ligament is about 0.13 % of the specimen thickness (14). In this study the region at the notch root of the Charpy-V specimen is modelled in plane strain, the rest in plane stress conditions. Figure 4 shows that the load vs. displacement-curve calculated with this combinated plane strain/plane stress model and using the same parameters as for the simulation of the tension test is in good agreement with the experimental one.

CONCLUSIONS

The material parameters for the strain rate hardening and the damage model can be extracted from the simulation of the smooth tensile specimen or the Charpy-V specimen. The deformation and fracture behaviour of the impacted

SENB specimen is well predicted using the micromechanical models. The adiabatic softening observed in the dynamic tension test plays only a small role in the tests of complex specimens where the region of large plastic deformation is relatively small. The results indicate that the critical void volume fraction f_c and the characteristic distance l_c are independent of the strain rate. In comparison with the J-integral concept the micromechanical models offer a wider range of application.

ACKNOWLEDEGMENTS

The authors gratefully acknowledge the financial support of the Preussen Elektra AG and of the German Science Foundation.

REFERENCES

(1) Krabiell, A., Dahl, W., Archiv für das Eisenhüttenwesen 52 (1981) 11, pp. 429-436
(2) Hesse, W., Ph.D. thesis, RWTH Aachen, 1986
(3) Harding, J., in: Impact Loading and Dynamic Behaviour of Materials, eds. Chiem, C.Y., Kunze, H.-D., Meyer, L.W., DGM Informationsgesellschaft, 1988, Vol. 1, pp. 23-42
(4) Stiebler, K., Kunze, H.-D., El-Magd, E., Nuclear Engineering and Design 127 (1991), pp. 85-93
(5) Needleman, A., Tvergaard, V., Int. J. Fract. 49 (1991), pp. 41-67
(6) Needleman, A., Tvergaard, V., J. Mech. Phys. Solids 35 (1987), pp. 151-183
(7) Sun, D.-Z., Voss, B. and Schmitt, W., in: Defect Assessment in Components - Fundamentals and Applications, ESIS/EGF9, eds. Blauel, J.G. and Schwalbe, K.-H., Mechanical Engineering Publications, London 1991, pp. 447-458
(8) Macherauch, E., Vöhringer, O., Z. Werkstofftechnik 9 (1978), pp. 370-391
(9) Pan, J., Saje, M., and Needleman, A., Int. J. Fracture 21 (1983), pp. 261-278
(10) Peirce, D., Shih, C.F., Needleman, A., Comp. Struct. 18 (1982), pp. 875-887
(11) Böhme, W., Sun, D.-Z., Schmitt, W., Hönig, A., in: Advances in Local Fracture/Damage Models for the Analysis of Engineering Problems, eds. Giovanola, J.H., and Rosakis, A.J. AMD-Vol. 137, ASME, 1992, pp. 203-216
(12) Sun, D.-Z., Hönig, A., Böhme, W., 24. Vortragsveranstaltung des Arbeitskreises Bruchvorgänge, Aachen, 1992
(13) Böhme, W., in Rapid Load Fracture Testing, eds. Chona R. and Corwin W.R., American Society for Testing and Materials, Philadelphia, ASTM STP 1130, 1992, pp. 92-103
(14) Riedel, H., Fracture at High Temperature, 1987

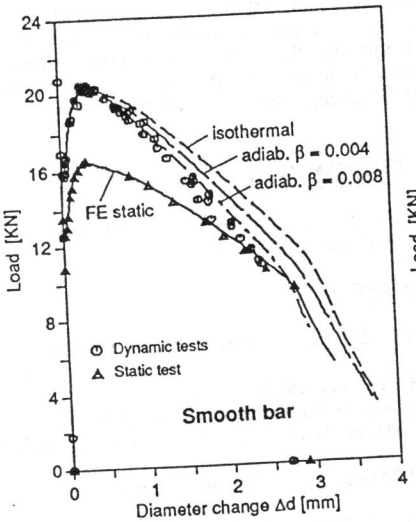

Figure 1 Experimental and numerical load vs. diameter change curves

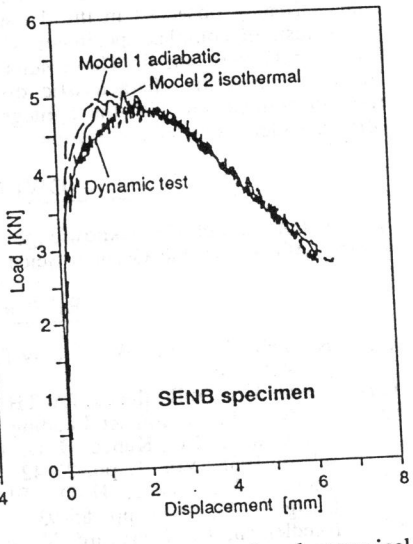

Figure 2 Experimental and numerical load vs. displacement curves

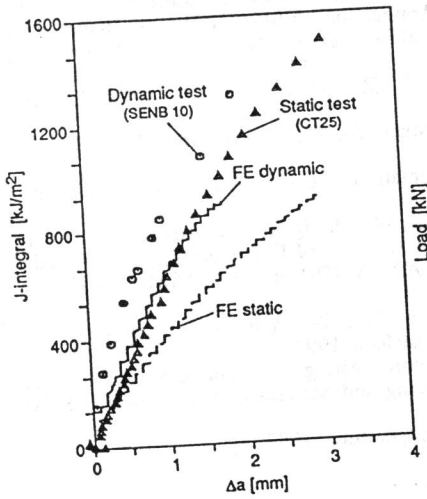

Figure 3 Experimental and numerical J_R-curves

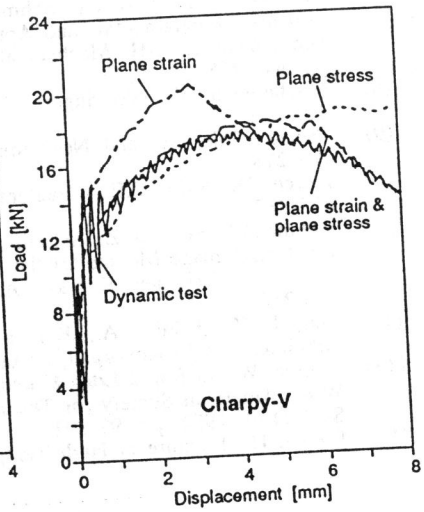

Figure 4 Experimental and numerical load vs. displacement curves